Supplement of Atmos. Chem. Phys., 18, 1395–1417, 2018
https://doi.org/10.5194/acp-18-1395-2018-supplement

Atmospheric Chemistry and Physics
Open Access
EGU

Supplement of

Emission or atmospheric processes? An attempt to attribute the source of large bias of aerosols in eastern China simulated by global climate models

Tianyi Fan et al.

Correspondence to: Tianyi Fan (fantianyi@bnu.edu.cn) and Xiaohong Liu (xliu6@uwyo.edu)

1. Mapping the MEIC emission inventory for CAM5

In addition to running CAM5 with the default AR5 emission inventory, we implement the new emission inventory MEIC into the model. We replace the default AR5 emission with the MEIC emission in China and keep the same as the AR5 emission elsewhere. We map the MEIC aerosols and precursor gases in different sectors to those required by the CAM5 chemistry and aerosol modules (Table S1). MEIC includes anthropogenic emissions in sectors named by power, industry, residential, and transportation, which correspond to the sectors of AR5 emission named by energy, industry, domestic, and transportation, respectively. Emissions due to shipping, agricultural waste burning and waste treatment as well as natural sources such as forest fires, grass fires and continuous volcanoes are not specified in the MEIC emission, so we keep them the same as those in the AR5 emission.

MEIC provides the emissions of aerosols and precursor gases including SO_2, black carbon (BC), organic carbon (OC), and non-methane volatile organic compounds (NMVOCs). Additional work is done to obtain a full set of species required by CAM5-MAM3 aerosol simulations, which includes SO_2, primary sulfate aerosol, BC, primary organic matter (POM), semi-volatile organic gas species (SOAG), dimethylsulfide (DMS), and number concentration in the accumulation and Aitken modes. These aerosols and precursor gases are emitted as surface or elevated sources. 2.5% (by molar) of the SO_2 emission is regarded as the primary sulfate aerosol emitted directly from sources following the Aerosol Comparisons between Observations and Models (AeroCom) protocol (Dentener et al., 2006) and the rest are emitted as SO_2. The energy and industrial SO_2 and primary sulfate are treated as elevated sources at 3 levels between 100 and 300 m, and their sources due to forest fires and grass fires are emitted in six vertical levels at 0 to 6 km (Dentener et al., 2006). SO_2 and primary sulfate from agriculture, domestic, transportation, waste, and shipping sectors are emitted at surface. Primary sulfate aerosols from domestic and transportation are put in the Aitken mode and those from other sectors are put in the accumulation mode (Liu et al., 2012).

The POM emission is assumed to be 1.4 times the OC emission in order to include the aerosol mass of other elements (i.e., oxygen, hydrogen, and nitrogen) (Seinfeld and Pandis, 1998). POM and BC from forest fires and grass fires are treated as elevated sources, while POM and BC from other sectors are treated as surface sources. All POM and BC aerosols are put in the accumulation mode. The SOAG species in CAM5-MAM3 is a lumped semi-volatile organic gas-phase species that can condense onto pre-existing aerosols to form SOA. Since the IPCC AR5 dataset does not provide biogenic volatile organic compound (VOC) emission, to simulate SOA in CAM5-MAM3, the SOAG emission is derived from the emission fluxes of five primary VOC categories (isoprene, monoterpenes, big alkanes, big alkenes, toluene) that are prescribed from the Model for OZone And Related chemical Tracers version 4 (MOZART-4) dataset (Emmons et al., 2010). In MOZART-4 the biogenic emissions of isoprene and monoterpenes are based on the Model for Emissions of Gases and Aerosols Emissions from Nature (MEGAN) (Guenther et al., 2006). The MEIC emission provides anthropogenic sources of the five VOC categories and the mapping table for lumping the MEIC VOC species to MOZART is provided by Li et al. (2014). Since the MEIC emission inventory does not provide biogenic sources of isoprene and monoterpenes, which are much larger than their

anthropogenic sources, we make the total emissions from anthropogenic and natural sources of these two species the same as those in the AR5 emission. The MEIC VOC emissions are then multiplied by the species molecular weights, the assumed mass yields (Liu et al., 2012), then divided by 1.4 (the POM/OC ratio) to derive the SOAG emission. We note that the SOAG emission is increased by a factor of 1.5 in CAM5 to account for the large uncertainty in SOA formation.

The number emission fluxes are calculated from the mass fluxes for sulfate, BC, and OC in a consistent way as those in the AR5 emission. The mass to number conversion is based on $E_{number} = E_{mass} / \left(\frac{\pi}{6} \rho {D_v}^3\right)$, where D_v is the volume-mean emitted diameter and ρ is the aerosol particle density (Liu et al., 2012). Since there are no corresponding sulfate, BC, or POM emissions from agricultural waste burning, waste treatment, forest fire, grass fire and continuous volcanoes in the MEIC emission, we use the number fluxes from the AR5 emission for these sectors.

Since the reanalysis data used for our offline meteorology is for year 2009, we obtain the emissions in 2009 by linear interpolation between year 2008 and 2010 for the MEIC emission and between year 2005 and 2010 for the AR5 emission.

Table S1. Mapping the MEIC emission to CAM5-MAM3 emission input data in China.

Species	Elevation	Sectors in CAM5 [a]	AR5 emission rates [e] (Gg/year)	Sectors in MEIC and mapping treatment [b]	MEIC emission rates [f] (Gg/year)
SO_2	Surface	dom	1692.2	res SO_2 x 97.5%	1593.3
		tra	289.0	tra SO_2 x 97.5%	101.1
		awb	29.9	-[c]	29.9
		wst	0.0	-	0.0
		shp	11.2	-	11.2
	Elevated	ene	7946.7	pow SO_2 x 97.5% [d]	4650.3
		ind	2937.5	Ind SO_2 x 97.5%	7826.3
		forest fire	7.0	-	7.0
		grass fire	1.4	-	1.4
		contvolc	0.0	-	0.0
Acc. mode sulfate	Surface	awb	0.8	-	0.8
		wst	0.0	-	0.0
		shp	0.3	-	0.3
	Elevated	ene	203.3	pow SO_2 x 2.5%	119.2
		ind	75.3	ind SO_2 x 2.5%	200.7
		forest fire	0.2	-	0.2
		grass fire	0.0	-	0.0
		contvolc	0.0	-	0.0

Ait. mode sulfate	Surface	dom	43.4	res SO_2 x 2.5%	40.9
		tra	7.4	tra SO_2 x 2.5%	2.6
	Elevated	contvolc	0.0	-	0.0
Total sulfur			**13246.0**		**14585.2**
BC	Surface	ene	20.5	pow BC	1.9
		ind	853.8	Ind BC	546.4
		dom	581.9	res BC	881.3
		tra	74.7	tra BC	286.1
		awb	43.9	-	43.9
		wst	6.4	-	6.4
		shp	0.3	-	0.3
	Elevated	fst	9.8	-	9.8
		grs	3.6	-	3.6
Total BC			**1595.0**		**1779.8**
POM	Surface	ene	93.6	pow OC x 1.4	0.0
		ind	1567.8	ind OC x 1.4	707.5
		dom	2314.5	res OC x 1.4	3778.8
		tra	129.5	tra OC x 1.4	148.3
		awb	292.8	-	292.8
		wst	9.0	-	9.0
		shp	0.5	-	0.5
	Elevated	fst	185.3	-	185.3
		grs	36.2	-	36.2
Total POM			**4629.0**		**5158.4**
SOAG	Surface	BIGALK	179.8	(pow + ind + tra + res ALK3, ALK4, ALK5)*molecular weight *mass yield*1.5^{g}	376.2
		BIGENE	33.6	(pow + ind + tran + res	91.4

				OLE2) *molecular weight *mass yield*1.5	
		TOLUENE	352.8	(pow + ind + tra + res ARO1, ARO2) *molecular weight *mass yield*1.5	1031.9
		ISOPRENE	712.6	-	712.6
		TERPENE	1289.6	-	1289.6
Total SOAG			**2568.3**		**3501.6**
DMS	Surface		8.2	-	8.2

[a] The AR5 sector abbreviations are dom (domestic), tra (transportation), ind (industry), ene (energy), wst (waste treatment), awb (agricultural waste burning), shp (shipping), fst (forest fire), grs (grass fire) and contvolc (continuous volcano).

[b] The MEIC sector abbreviations are res (residential), tra (transportation), ind (industry), and pow(power).

[c] "-" means that the species in the sector is the same as AR5 emission.

[d] The elevated energy and industry emissions are emitted in mass fraction of 15.5% , 75.1%, and 9.4% at approximately 30, 130, and 280 meters.

[e] The masses of SO_2, sulfate and DMS are in unit of Gg of Sulfur per year in China. The unit of BC mass is Gg of Carbon per year and the units of POM and SOAG mass are Gg of POM per year, which is assumed to be 1.4 times OC (or Carbon) mass.

[f] The units are the same as in the column of AR5 emission rates.

[g] Atmoic compositions for BIGALK, BIGENE, TOLUENE are C_5H_{12}, C_4H_8, and $C_6H_5(CH_3)$, respectively. Mass yields of BIGALK, BIGENE, and TOLUENE are 5%, 5%, 15%, respectively.

2. Comparing MEIC and AR5 emission inventories

In East Asia the AR5 emission inventory incorporates the Regional Emission inventory in ASia (REAS) dataset (Ohara et al., 2007). The IPCC AR5 emission inventory has been widely used for global and regional climate studies (Giorgi et al., 2009; Jones et al., 2011; Shindell et al., 2013). Figure S1 compares the MEIC and AR5 emission inventories in China. The spatial distributions of the two emission inventories are generally consistent. The MEIC emission rates in China are 14.59 Tg Sulfur (S)/year, 1.78 Tg Carbon (C) yr^{-1}, 5.16 C Tg yr^{-1}, 3.50 C Tg yr^{-1} for SO_2 (including 5% mass contributed by the primary sulphate that is directly emitted), BC, POM, and SOAG, respectively (Table S1) and are 10.11%, 11.59%, 11.44%, and 36.34% higher than the AR5 emissions, respectively. The emissions are mostly concentrated in eastern China where the MEIC emission rates are 13.60 Tg S/year, 1.59 Tg C/year, 4.38 Tg C/year, 2.86 C Tg/year for SO_2 (including primary sulfate), BC, POM, and SOAG, respectively, which are 12.57%, 13.35%, 12.04%, and 46.88% higher than the AR5 emissions, respectively. SO_2, BC and POM emissions in MEIC are generally higher in northern China and the Sichuan Basin than those in AR5, whereas they are lower in Southern China. The SOAG are higher in MEIC than AR5 in most part of eastern China, especially in southern China. Both emission inventories highlight the emission "hotspots" in the Jing-Jin-Ji region, Henan, Shangdong, Jiangsu Provinces, and the Sichuan Basin. SO_2 industrial emission is the major contributor to the "hotspots". Industrial and domestic emissions result in the high POM and BC emission in these "hotspots". Dust emission is identical between the two runs since the same constrained surface wind speed drives the dust emission.

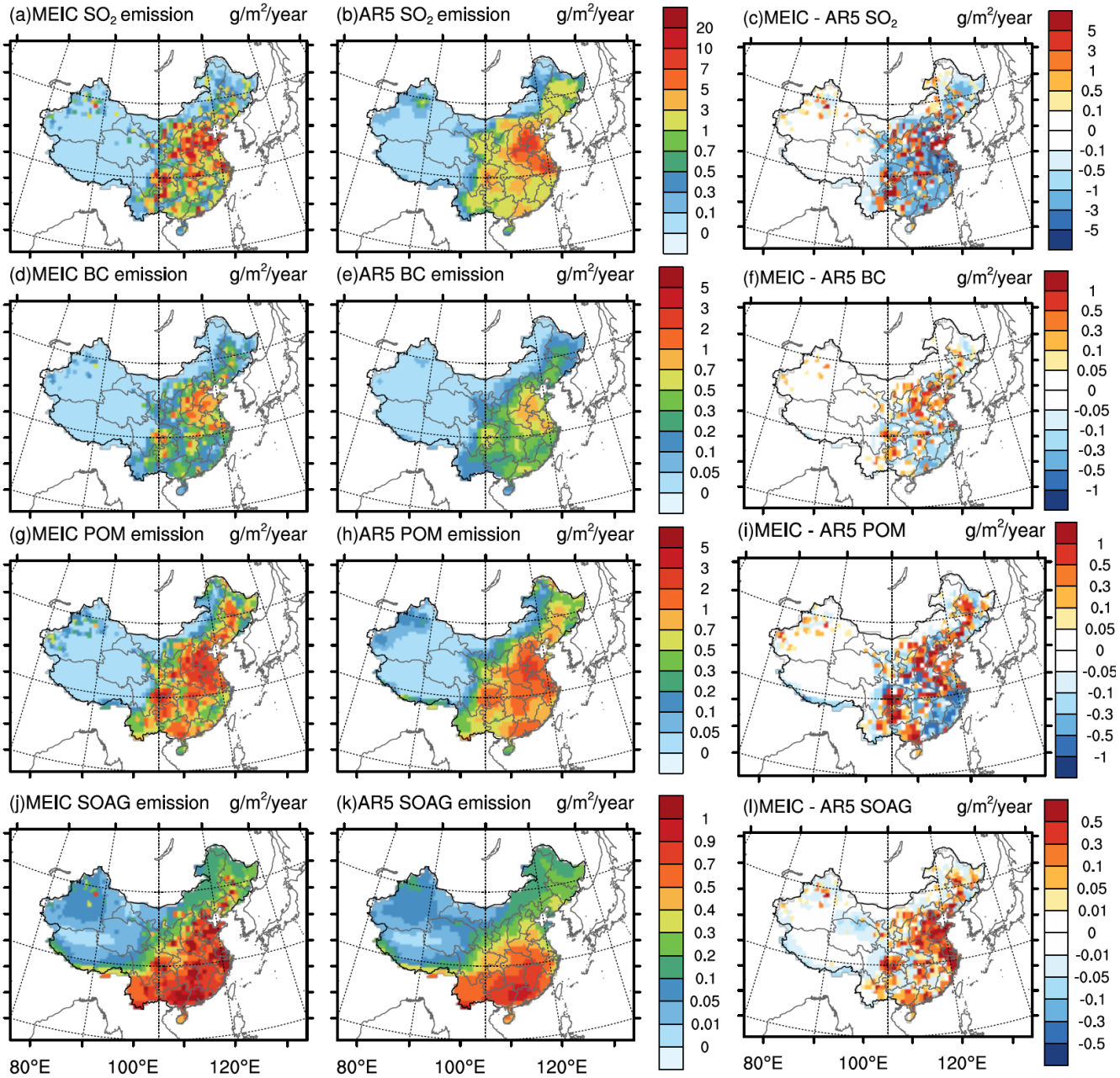

Figure S1. The spatial distributions of the MEIC emission, the AR5 emission and their difference for (a)-(c) SO_2, (d)-(f) BC, (g)-(i) POM, and (j)-(l) SOAG of year 2009 in China.

3. Comparing MEIC and CEDS emission inventories

The Community Emission Data System (CEDS) is newly released and is intended for use in CMIP6 (Hoesly et al., 2017). According to Hoesly et al. (2017), CEDS follows a completely different approach than the country-level emission inventory, such as MEIC. A global default dataset was first compiled using activity data (e.g., energy consumption), emission factors, and emission inventories. Then a "mosaic" strategy is used to scale the default emission estimates to authoritative country-level inventories. For China the CEDS dataset is scaled to MEIC for year 2008, 2010, and 2012 (Li et al., 2017) for most chemical species, except that BC and OC emissions are calculated using SPEW data (Bond et al., 2007). Gridded data are finally constructed using normalized spatial proxy (EDGAR gridded emission or HYDE population) distributions for each country. In terms of seasonality, the monthly fractions used in CEDS are from ECLIPSE project and do not change by year. Since our study is confined to eastern China, we do not consider smoothness with the surrounding area, MEIC is adequate and even better in seasonality than CEDS.

The overall spatial distributions of MEIC and CEDS are similar, but local difference exists between the two inventories (Figure S2). Seasonal variations also show similar trend for BC and OC (Figure S3). However, significant difference can be found for SO_2. The magnitude of SO_2 emission in MEIC is about 20% lower than that in CEDS. Compared with MEIC, CEDS SO_2 emission shows smoother seasonal cycle characterized by high emission rates in winter and low emission rates in the summer. By examining the emission rates by sectors, we find that all sectors in MEIC SO_2 emission are smaller than CEDS (Table S2). Particularly, the energy/power sector produced SO_2 in MEIC (4853.8 Gg S/year) is 32% lower than that in CEDS (7171.2 Gg S/year). We also noticed that BC and OC emissions in the MEIC power/energy sector (2.0 Gg C/year and 0.035 Gg C/year, respectively) are much smaller than BC and OC emission in CEDS (654.6 Gg C/year and 1115.9 Gg C/year, respectively). This could be due to the use of SPEW data (Bond et al., 2007) for BC and OC emissions in CEDS (Hoesly et al., 2017). Generally, the CEDS emission for eastern China is comparable with MEIC since CEDS is scaled to country-level inventories. Without improvements in the aerosol process, the similar low-bias over eastern China in CMIP5 GCMs are expected in CMIP6.

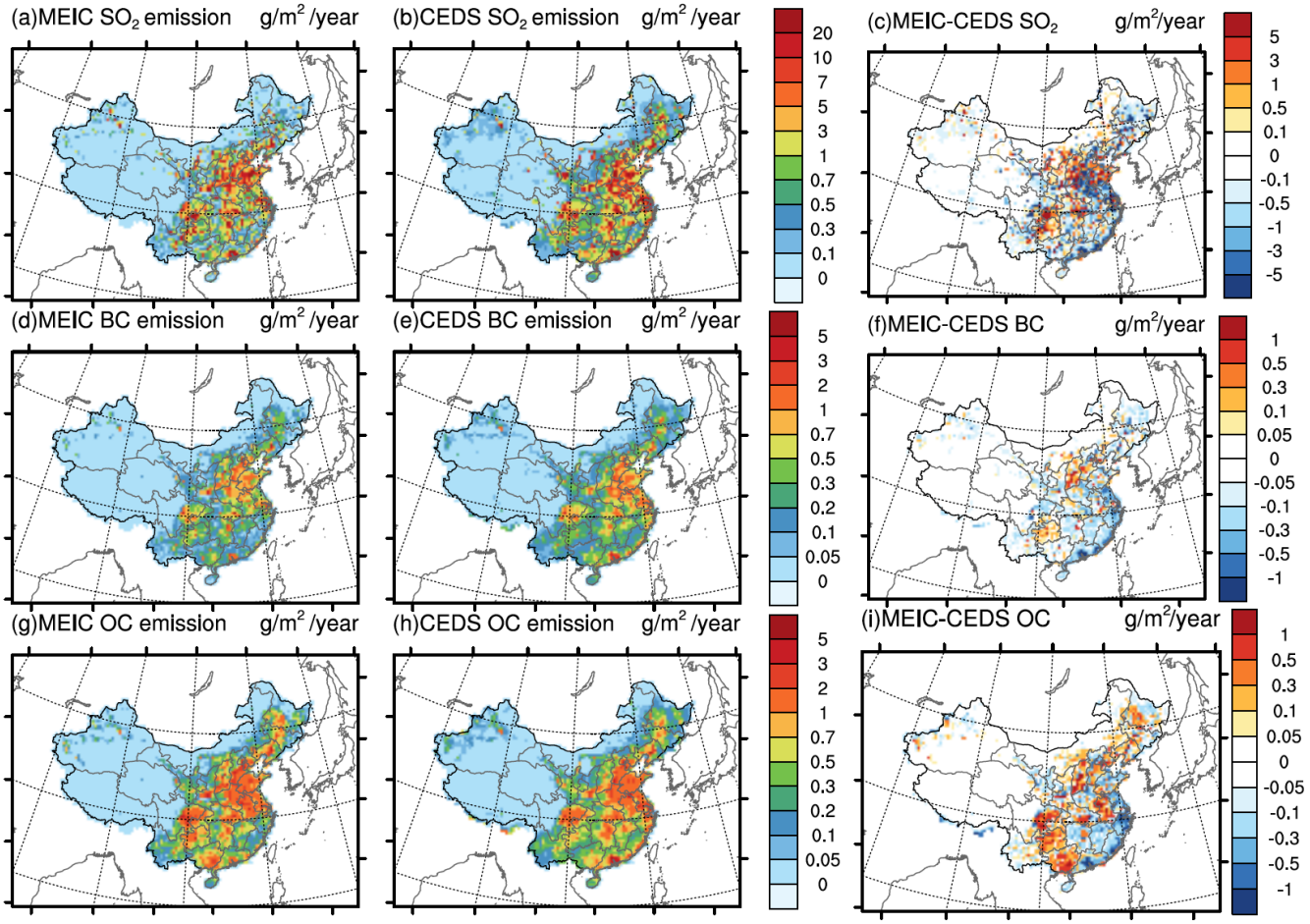

105 **Figure S2. The spatial distributions of the MEIC emission, the AR5 emission and their difference for (a)-(c) SO_2, (d)-(f) BC, (g)-(i) POM of year 2009 in China.**

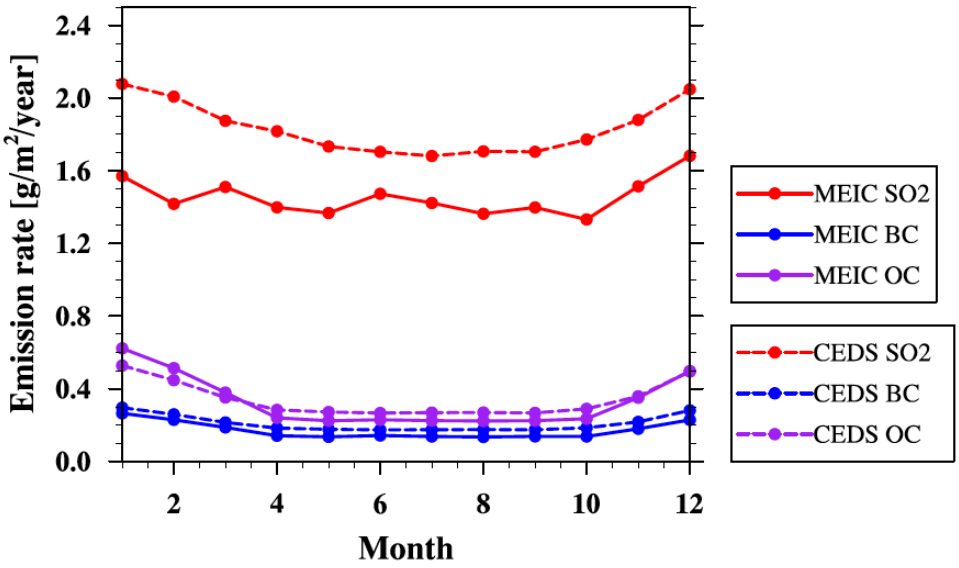

Figure S3. Seasonal variations of sulfate, BC, and POM in the MEIC emission and the CEDS emission in China for year 2009.

110

Table S2. Statistics of the anthropogenic emission of SO2 (Gg S/year), BC(Gg C/year), and OC(Gg C/year) in MEIC and CEDS inventories for year 2009 in China

Species/Sectors		MEIC	CEDS
SO_2	industry	8273.5	9399.9
	power	4853.8	7171.2
	residential	1649.2	1950.0
	transportation	106.6	237.4
	total	14883.1	18758.4
BC	industry	560.8	277.7
	power	2.0	654.6
	residential	893.8	962.3
	transportation	293.5	245.0
	total	1750.1	2139.5
OC	industry	517.8	232.4
	power	0.035	1115.9
	residential	2743.9	2033.9
	transportation	108.9	107.0
	total	3370.6	3489.1

4. Observations of aerosol chemical compositions in China

Table S3. The observations of surface concentrations of chemical species in $PM_{2.5}$ over eastern China in 2009 and 2010.

Locations	Coordinates	Time	Chemical species	References	Location type
Harbin	45.82°N, 126.56°E	Aug-Dec, 2010	SO_4,BC,OC	Huang et al.[2014]	urban
Chengde	40.95°N, 117.96°E	April/July/Oct, 2009;Jan, 2010	SO_4,BC,OC	Zhao et al. [2013]	urban
Shangdianzi	38.04°N, 114.51°E	April/July/Oct, 2009;Jan, 2010	SO_4,BC,OC	Zhao et al. [2013]	rural
Beijing1	39.93°N, 116.30°E	April/July/Oct, 2009;Jan, 2010	SO_4,BC,OC	Zhao et al. [2013]	urban
Beijing2	39.99°N, 116.30°E	April/July/Oct, 2009;Jan, 2010	SO_4,BC,OC	Zhang et al. [2013]	urban
Tianjin	39.08°N, 117.20°E	April/July/Oct, 2009;Jan, 2010	SO_4,BC,OC	Zhao et al. [2013]	urban
Shijiazhuang	38.04°N, 114.51°E	April/July/Oct, 2009;Jan, 2010	SO_4,BC,OC	Zhao et al. [2013]	urban
Zhengzhou	34.80°N, 113.50°E	April/July/Oct, 2009;Jan, 2010	SO_4,BC,OC	Geng et al. [2013]	urban
Shanghai	31.18°N, 121.42 °E	Jan, 2009	SO_4,BC,OC	Feng et al. [2012]	urban
	31.25°N, 121.46 °E	Oct, 2005; Jan/Apr/July,2006	SOA	Feng et al. [2009]	urban, suburban
Wuhan	30.50°N, 114.3 °E	Aug 2012- July 2013	SOA	Zhang et al. [2015]	urban, suburban
Chengdu*	30.65°N, 104.00°E	Apr/May, 2009	SO_4,BC,OC	Tao et al., [2013]	urban
Xiamen	24.58°N, 118.09°E	Jun,2009-May,2010	SO_4,BC,OC	Zhang et al. [2012]	urban
Guangzhou	23.10°N, 113.3°E	April/July/Oct, 2009;Jan, 2010	SO_4,BC,OC	Tao et al. [2014]	urban
	23.70°N, 113.6°E	Mar,2012-Mar,2013	SOA	Lai et al.[2015]	rural

* *Tao et al.* [2013] highlights the importance of the dust and biomass burning episodes to the chemical composition of PM2.5. We use their data on non-episodic days.

5. Observations of aerosol direct radiative effects in China

Table S4. Aerosol direct radiative effects (ADREs) at TOA, surface (SFC), and within the atmosphere (ATM) in different regions and periods in China.

Region	References	Period	TOA ($W\ m^{-2}$)	SFC ($W\ m^{-2}$)	ATM ($W\ m^{-2}$)
CSHNET	Li et al. (2010)	Jan.-Dec. 2005			
Ansai (36.85°N, 109.31°E)	Xin et al. (2007)		-0.46	-12.08	12.58
Beijing (39.97°N, 116.37°E)			-3.30	-30.60	27.30
Beijing Forest (39.96°N, 115.43°E)			-0.91	-7.59	6.66
Changbai Mt. (42.40°N, 128.63°E)				-6.67	6.82
Eerduosi (39.48°N, 110.18°E)				-6.02	6.02
Fengqiu (35.00°N, 114.40°E)			-0.12	-14.34	14.22
Fukang (44.28°N, 87.92°E)			2.03	-5.80	7.80
Haibei (37.45°N, 101.32°E)					3.57
Hailun (47.43°N, 126.63°E)				-6.78	7.06
Jiaozhou Bay (35.90°N, 120.18°E)			-2.81	-24.12	21.31
Lanzhou (36.07°N, 103.82°E)				-22.29	21.94
Lhasa (29.67°N, 91.33°E)				-4.28	4.83
Sanjiang (47.58°N, 133.52°E)			0.93	-6.92	7.85
Shanghai (31.12°N, 121.75°E)				-24.26	25.09
Shapotou (37.45°N, 104.95°E)				-7.45	7.42
Shenyang (41.52°N, 123.63°E)				-14.58	16.15
Taihu (31.40°N, 120.22°E)			-2.64	-15.79	13.15
Taoyuan (28.92°N, 111.45°E)			0.35		19.95
Xianghe (39.75°N, 116.96°E)			-1.28	-28.78	27.50
Yanting (31.27°N, 105.45°E)			1.26	-29.61	30.78
Xishuangbanna(21.9°N, 101.27°E)			2.40	-18.17	20.55
Others					
Xianghe (39.75°N, 116.96°E)	Li et al. (2007)	Jan.-Dec. 2004-2005		-24	
Beijing (39.98°N, 116.38°E)	Xia et al. (2007a)	Dec.-Feb.	-8.0	-20.3	

		Mar.-May	-13.9	-46.1	
		Jun.-Aug.	-13.5	-45.6	
		Sep.-Nov.	-10.7	-30.0	
		2001-2005			
Liaozhong (41.50°N, 120.70°E)	Xia et al. (2007b)	Mar.-May 2005		-30	
Taihu (31.70°N, 120.36°E)	Xia et al. (2007c)	Jan.-Dec. 2005-2006	0	-38.4	
Nanjing (32.05°N, 118.78°E)	Zhuang et al. (2014)	Jan.-Dec. 2011-2012	-6.9	-21.3	
SACOL (35.95°N, 104.10°E)	Liu et al. (2011)	May 2009	-7.78	-38.45	30.68

6. Figures

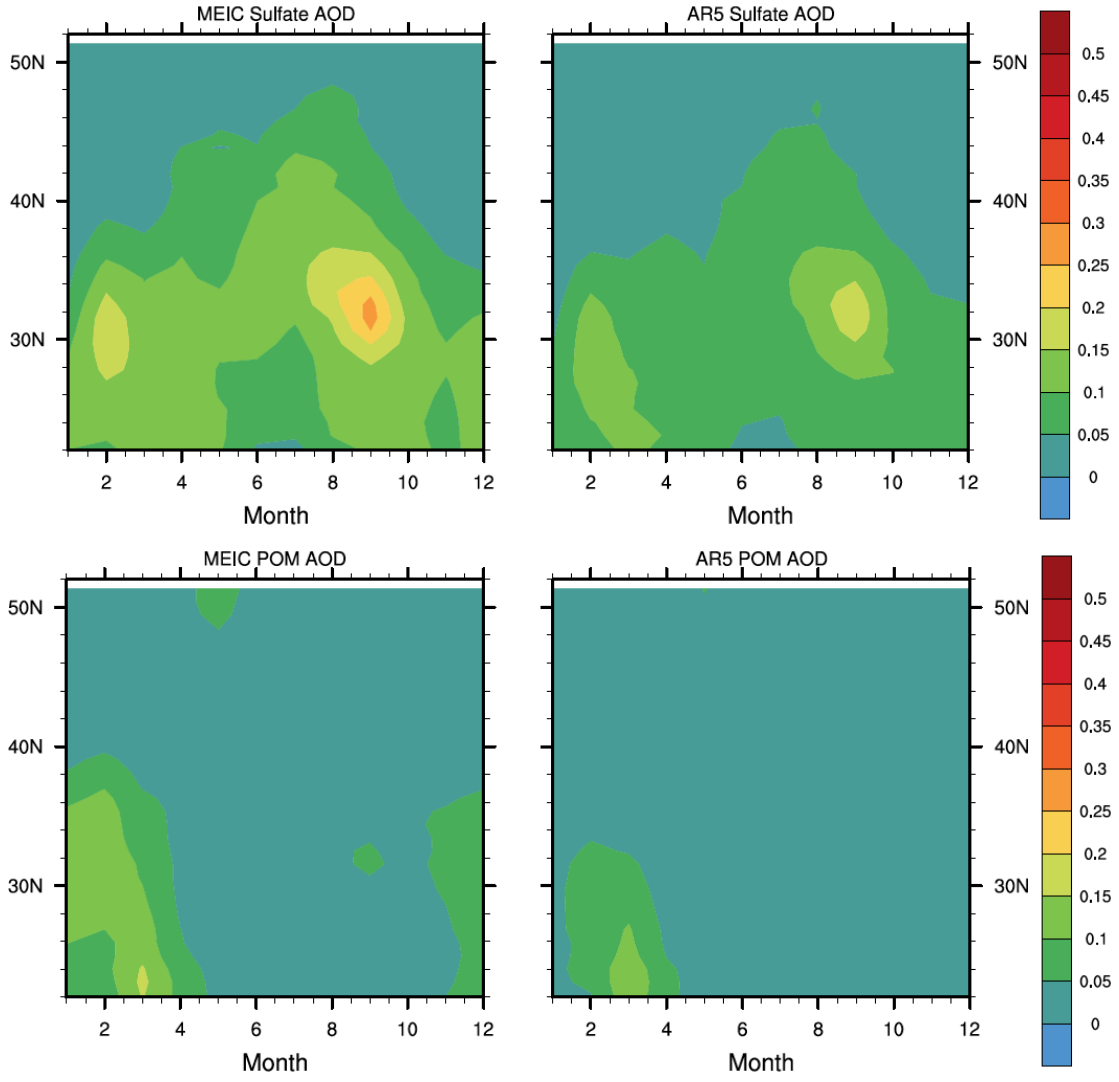

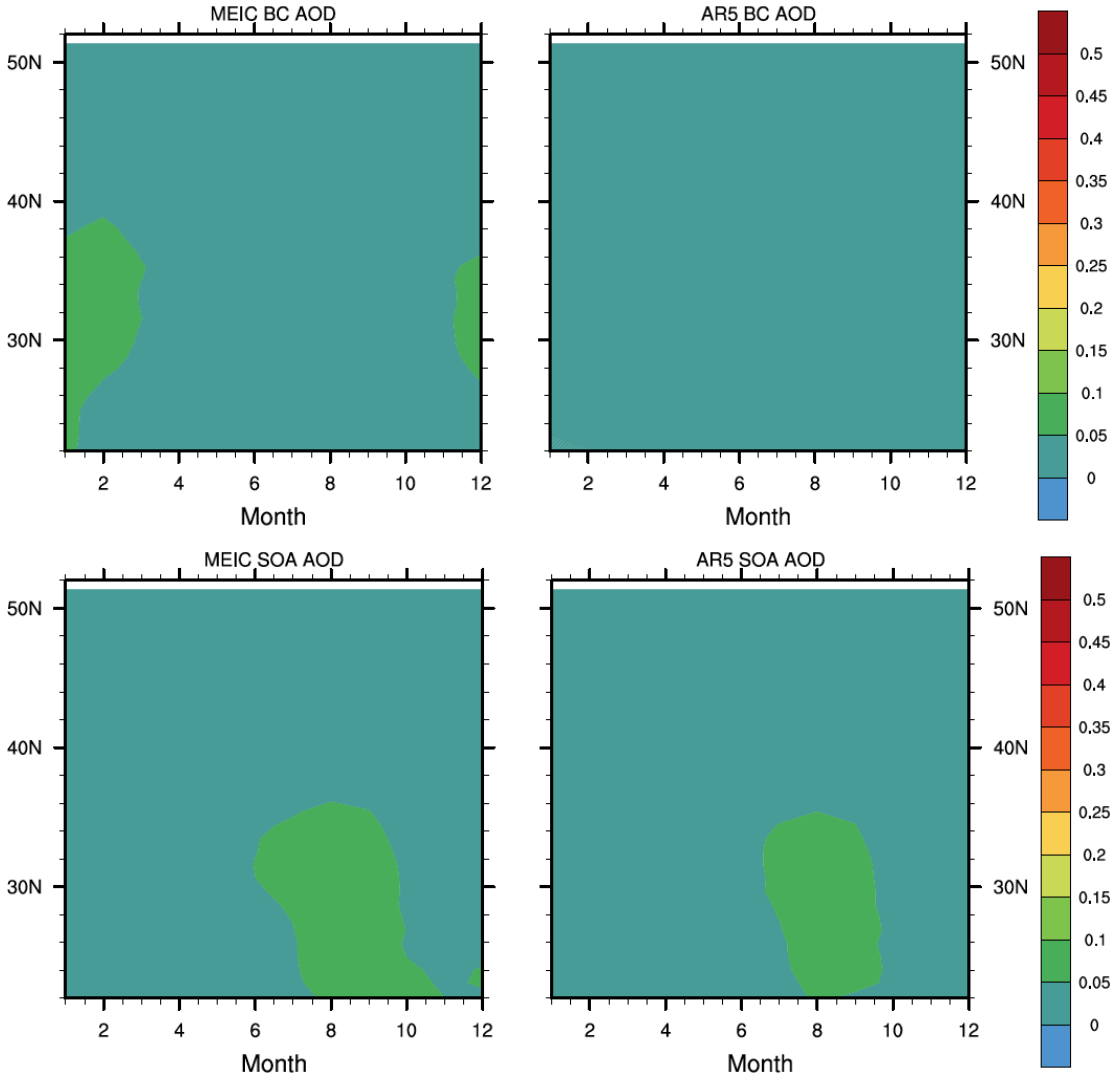
MEIC BC AOD
AR5 BC AOD
MEIC SOA AOD
AR5 SOA AOD
50N
40N
30N
2
4
6
8
10
12
Month
0.5
0.45
0.4
0.35
0.3
0.25
0.2
0.15
0.1
0.05
0

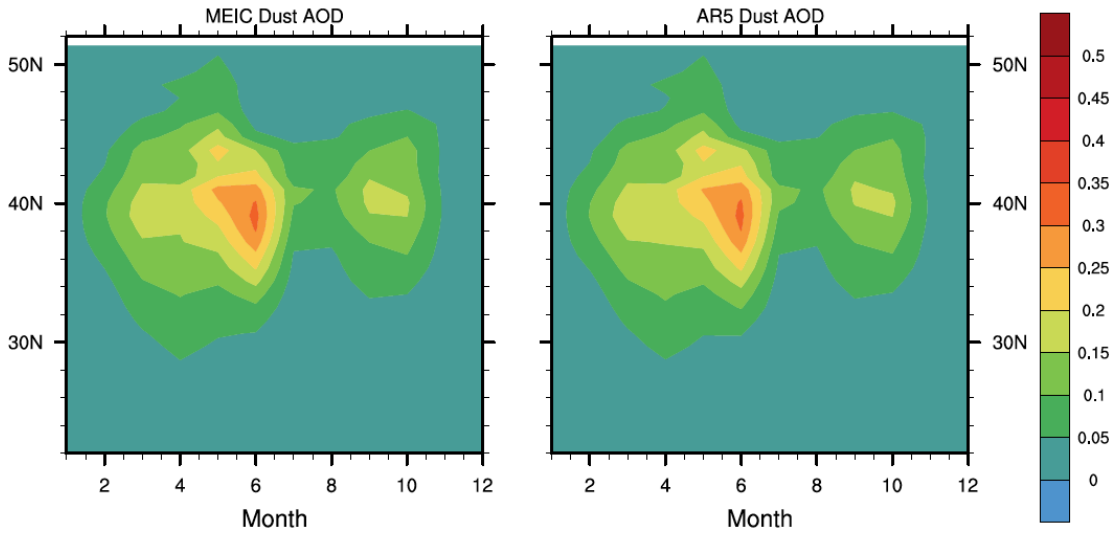

Figure S4. The seasonal variation of longitudinal averaged (100°E-124°E) AOD at 550 nm by aerosol components (dust, sulphate, BC, POM, and SOA from top to bottom) simulated by CAM5-MAM3 using the MEIC emission (left column) and the AR5 emission (the right column).

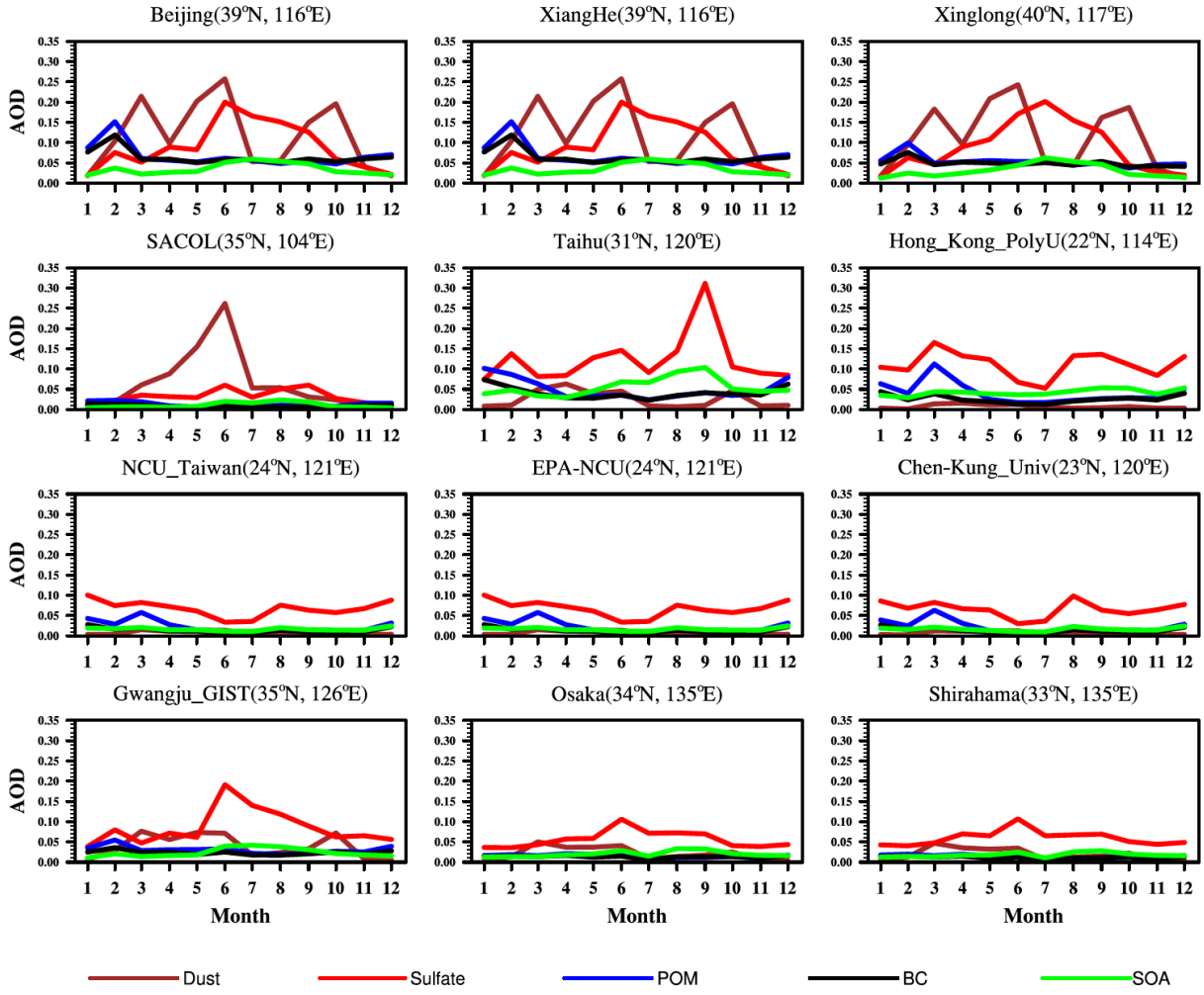

Figure S5. Seasonal variations of monthly mean AODs by aerosol species at 12 AERONET sites simulated by CAM5 using the MEIC emission inventory.

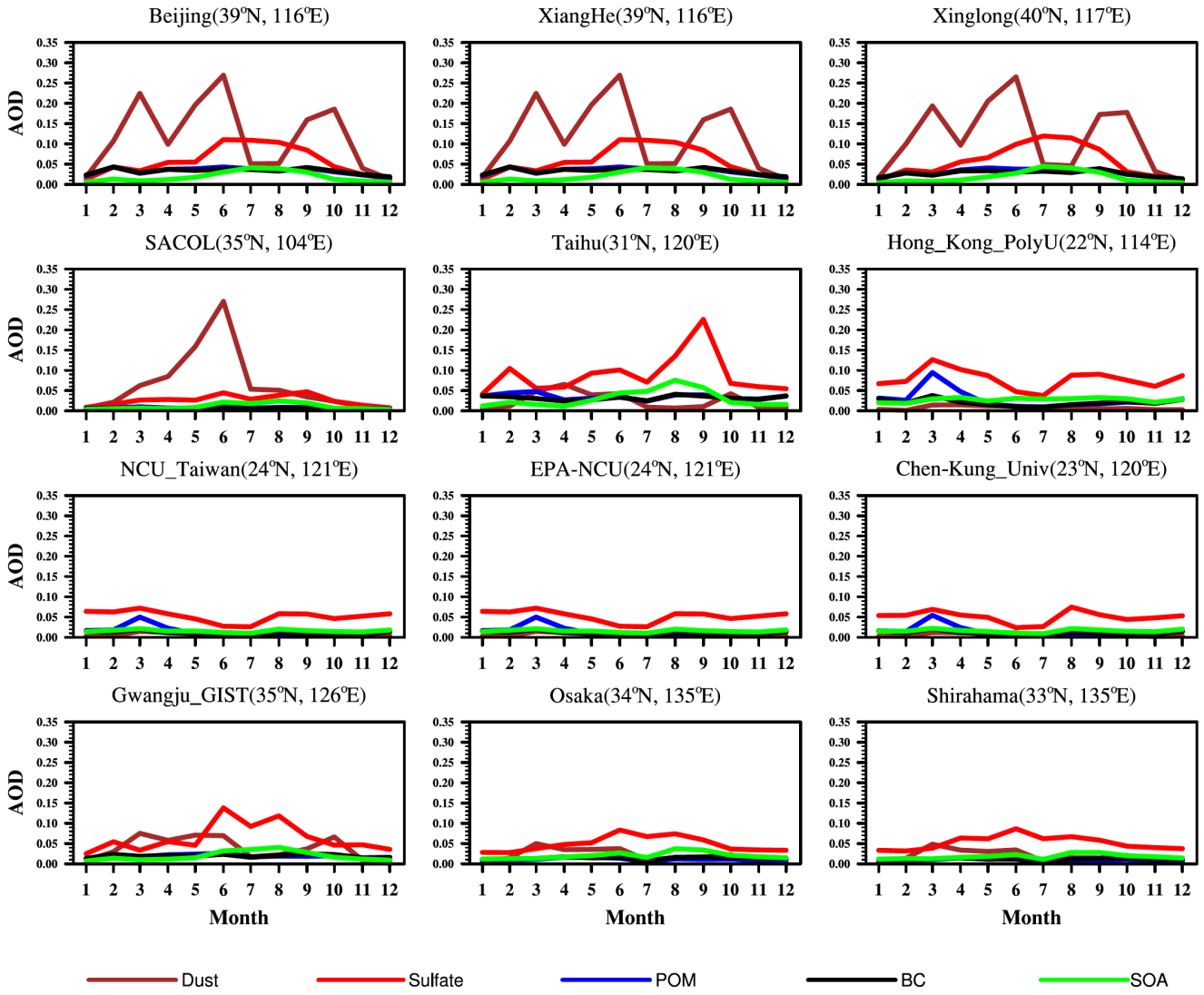

Figure S6. Same as Figure S5 but using the AR5 emission inventory.

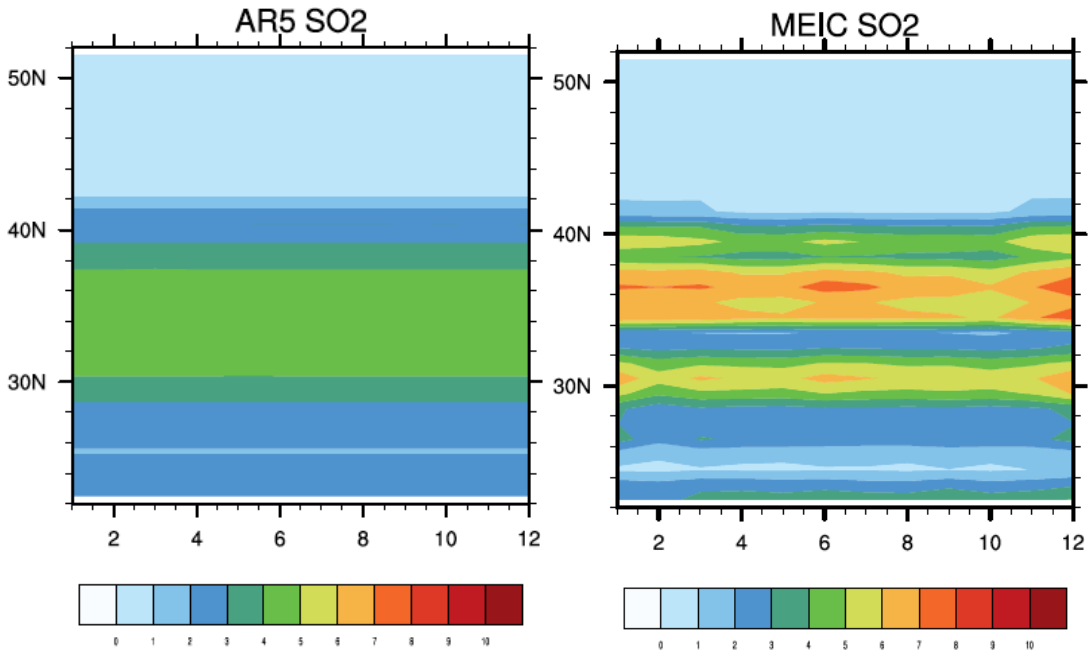

Figure S7. The seasonal variation of longitudinal averaged SO_2 emission from AR5 and MEIC [g S/m^2/year].

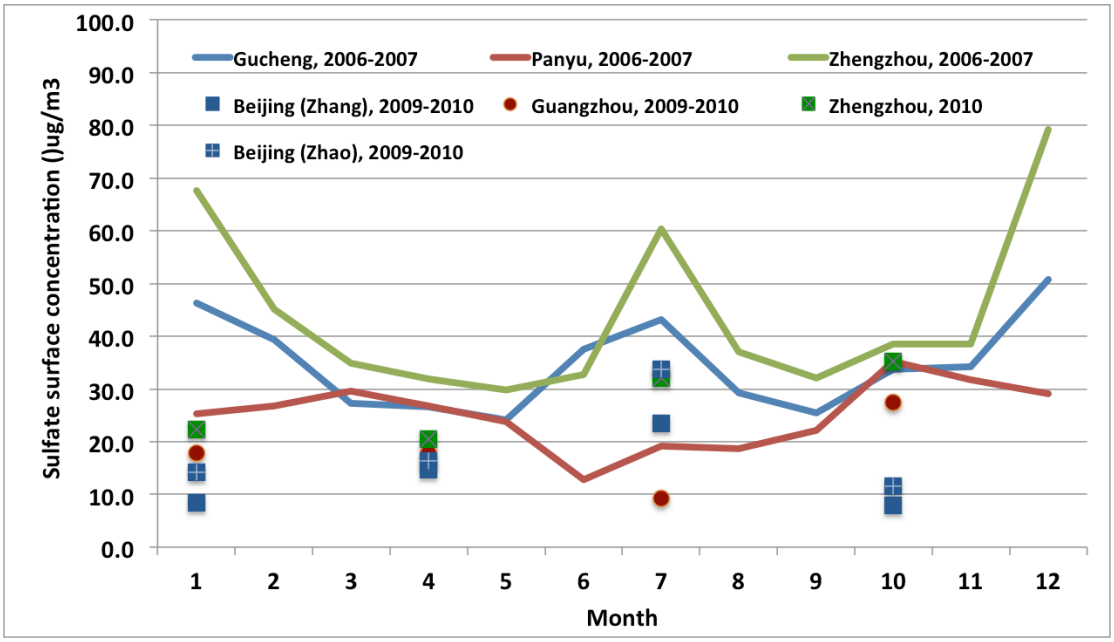

Figure S8. Seasonal variations of surface concentration of sulfate at three locations (Gucheng, Panyu, and Zhengzhou) from CAWNET from 2006 to 2007. For comparison, the observations near the three CAWNET locations in our study (Beijing, Guangzhou, Zhengzhou) from 2009 to 2010 are also shown in dots.

7. Decadal trend of emission from 2002 to 2012 over eastern China

Figure S7 shows the MEIC's SO_2, BC, and OC emission trends from 2002 to 2012 in eastern China. Since spatially-gridded MEIC emission data are only available for 2008, 2010, and 2012, we obtained the spatial distribution and seasonal variation of other years by scaling the spatial-temporal variation of the emission in 2008 with the annual mean emission rates in these years. The annual mean emission rates of each species (SO_2, BC, and OC) are estimated by the MEIC development team. Each species in different sectors (power, energy, residential, and transportation) has a different scaling factor. The annual trends are consistent with other researches (Lu et al., 2011; Lei et al., 2009) although the absolute values are different. We use the MEIC estimations of the decadal trend because it is based on the same algorithm and database of fuel usage (i.e., China Energy Statistical Yearbook) as the MEIC emission that we used for 2009.

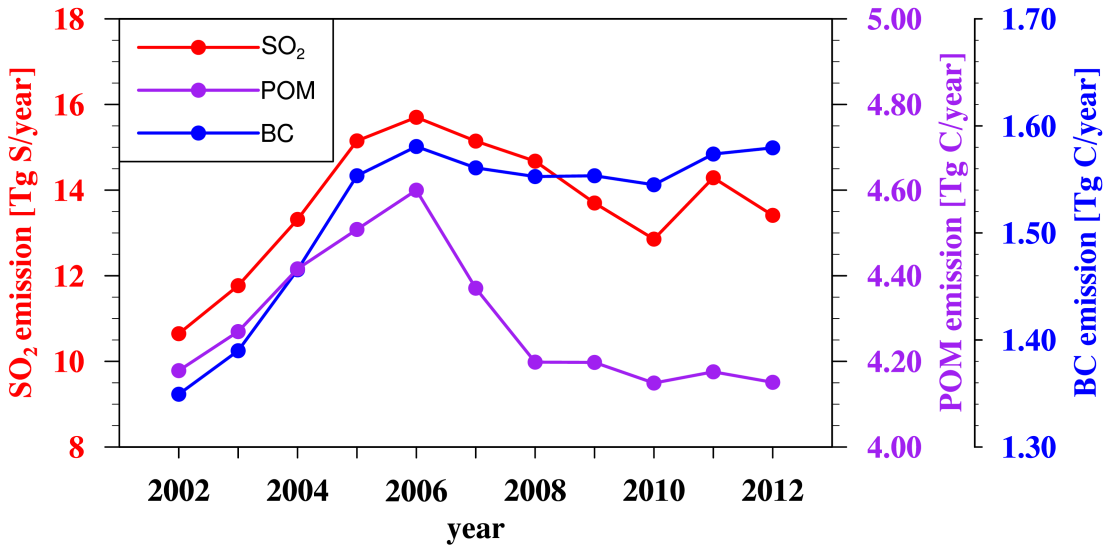

Figure S9. The change of emission rates of SO_2, BC, and POM from year 2002 to 2012 over eastern China.

8. Aerosol-meteorological interaction in the fast processes

In the nudged simulations, only horizontal winds are nudged toward the reanalysis with a relaxation time scale of 6 hours. This approach facilitates direct evaluation of model aerosols against observations at particular times and locations when the errors (and uncertainties associated with natural variability) in the modeled large-scale circulation is minimized. **Temperature and moisture are not nudged in this study.** As evaluated in Zhang et al (2014), nudging temperature and moisture creates a large perturbation to the model state, resulting in unrealistic behaviour for cloud and convection parameterizations because these parameterizations are calibrated based on the free-running model climate. Because winds are constrained, the advection of heat and moisture are constrained to some degree (when the difference in local temperature and moisture between two simulations is small), but local source and sink terms for atmospheric temperature and moisture are computed according to the model fast processes (e.g., cloud processes) and land processes (climatological sea surface

temperatures are prescribed in the two simulations). The changes in atmospheric temperature and moisture can in turn influence the gas- and aqueous-phase chemistry and aerosols.

Our analysis shows that there are small differences in the temperature ($\Delta T < 1$ K) and moisture ($\Delta RH < 3\%$) between the MEIC run and the AR5 run in Figures 9 and 11 as shown in the figure below. However, the differences are almost indiscernible compared to seasonal variation, which is about 30-40 K in northern China and about 20 K in southern China (red curves in the second column of Figure 9). The temperature and moisture differences between the two simulations are indiscernible in Figure 9. The small changes in temperature and moisture reflect the differences in aerosol effects on meteorology through fast processes between the two aerosol emissions. Total impacts on temperature and moisture can be assessed by using a fully coupled, free-running earth system model, which is beyond the scope of this study (since we focus on the aerosol radiative forcing).

Next, we show that this temperature difference is reasonable. The magnitude of the temperature difference is the result of change of equilibrium state from AR5 to MEIC aerosol, which can be regarded as a radiative forcing (ΔF), i.e., the energy change induced by different aerosol loadings between the two runs. The radiative forcing ΔF is calculated from difference between ADREs in the two simulations (-10.34 Wm^{-2} for the AR5 run and -12.76 Wm^{-2} for the MEIC run, see Table 2), which is -2.42 Wm^{-2}. We can obtain the change of surface temperature (ΔT_s) by multiplying ΔF with the climate sensitivity, α,

$$\Delta T_s = \alpha \Delta F$$

The climate sensitivity is estimated to be ~4 K with a doubling of CO_2 (3.7 Wm^{-2}) for CAM5. Therefore, the direct response of surface temperature, in the absence of the ocean feedbacks, is about 1 K.

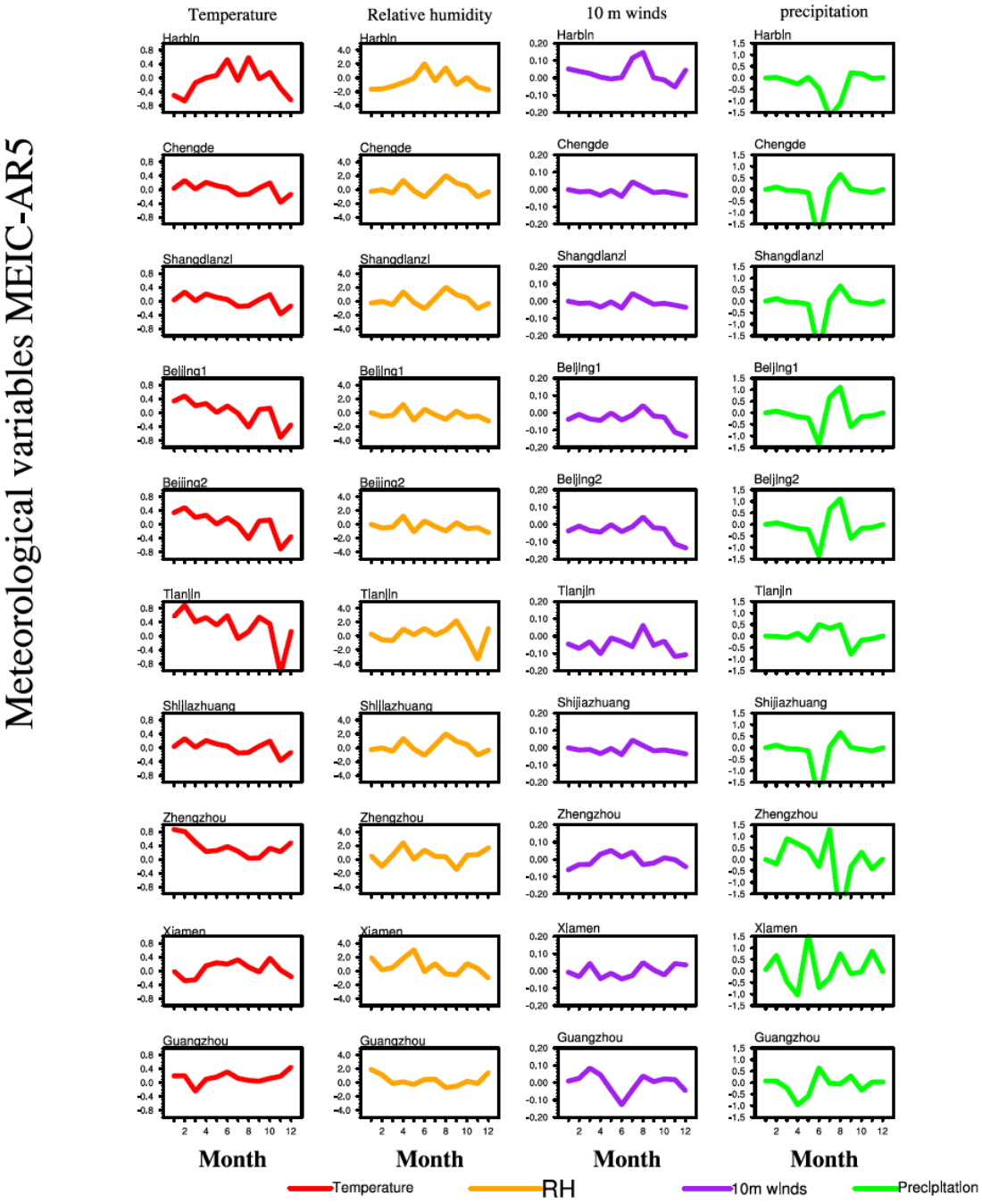

190 **Figure S10. Seasonal variation of the differences between the meteorological variables due to atmospheric and land fast processes introduced by aerosol differences between the MEIC and AR5 simulations in 10 locations in eastern China from north to south. From left to right: temperature (unit: K), relative humidity (unit: %), 10-m winds (unit:ms^{-1}), precipitataion (unit: mm/day).**

References

Bond, T. C., Bhardwaj, E., Dong, R., Jogani, R., Jung, S., Roden, C., Streets, D. G. and Trautmann, N. M.: Historical emissions of black and organic carbon aerosol from energy-related combustion, 1850-2000, Glob. Biogeochem. Cycles, 21(2), doi:10.1029/2006GB002840, 2007.

Dentener, F., Kinne, S., Bond, T., Boucher, O., Cofala, J., Generoso, S., Ginoux, P., Gong, S., Hoelzemann, J. J., Ito, A., Marelli, L., Penner, J. E., Putaud, J.-P., Textor, C., Schulz, M., van der Werf, G. R., and Wilson, J.: Emissions of primary aerosol and precursor gases in the years 2000 and 1750 prescribed data-sets for AeroCom, Atmos. Chem. Phys., 6(12), 4321-4344, 2006.

Emmons, L. K., Walters S., Hess, P. G., Lamarque, J.-F., Pfister, G. G., Fillmore, D., Granier, C., Guenther, A., Kinnison, D., Laepple, T., Orlando, J., Tie, X., Tyndall, G., Wiedinmyer, C., Baughcum, S. L., and Kloster, S.: Description and evaluation of the Model for Ozone and Related chemical Tracers, version 4 (MOZART-4), Geosci. Model Dev., 3(1): 43-67, 2010.

Feng, J., Sun, P., Hu, X., Zhao, W., Wu, M., and Fu, J.: The chemical composition and sources of $PM_{2.5}$ during the 2009 Chinese New Year's holiday in Shanghai, Atmos. Res., 118, 435-444, 2012.

Feng, Y., Chen, Y., Guo, H., Zhi, G., Xiong, S., Li, J., Sheng, G., and Fu, J.: Characteristics of organic and elemental carbon in $PM_{2.5}$ samples in Shanghai, China, Atmos. Res., 92(4), 434-442, 2009.

Geng, N., Wang, J., Xu, Y., Zhang, W., Chen, C., and Zhang, R.: $PM_{2.5}$ in an industrial district of Zhengzhou, China: chemical composition and source apportionment, Particuology, 11(1), 99-109, 2013.

Giorgi, F., Jones, C., and Asrar, G. R.: Addressing climate information needs at the regional level: the CORDEX framework, WMO Bulletin, 58(3), 175–183, 2009.

Guenther, A., Karl, T., Harley, P., Wiedinmyer, C., Palmer, P. I., and Geron, C.: Estimates of global terrestrial isoprene emissions using MEGAN (Model of Emissions of Gases and Aerosols from Nature), Atmos. Chem. Phys., 6, 3181–3210, 2006.

Hoesly, R. M., Smith, S. J., Feng, L., Klimont, Z., Janssens-Maenhout, G., Pitkanen, T., Seibert, J. J., Vu, L., Andres, R. J., Bolt, R. M., Bond, T. C., Dawidowski, L., Kholod, N., Kurokawa, J.-I., Li, M., Liu, L., Lu, Z., Moura, M. C. P., O'Rourke, P. R., and Zhang, Q.: Historical (1750–2014) anthropogenic emissions of reactive gases and aerosols from the Community Emission Data System (CEDS), Geosci. Model Dev. Discuss., https://doi.org/10.5194/gmd-2017-43, 2017.

Huang, L. and Wang, G.: Chemical characteristics and source apportionment of atmospheric particles during heating period in Harbin, China, J. Environ. Sci., 26(12), 2475-2483, 2014.

Jones, C., Giorgi, F., and Asrar. G.: The coordinated regional downscaling experiment: CORDEX An international downscaling link to CMIP.CLIVAR Exchanges, 16(2), 34–40, 2011.

Lai, S., Zhao, Y., Ding, A., Zhang, Y., Song, T., Zheng, J., Ho, K. F., Lee, S.-C., and Zhong, L.: Characterization of $PM_{2.5}$ and the major chemical components during a 1-year campaign in rural Guangzhou, Southern China, Atmos. Res., 167, 208-215, 2016.

Li, M., Zhang, Q., Streets, D. G., He, K. B., Cheng, Y. F., Emmons, L. K., Huo, H., Kang, S. C., Lu, Z., Shao, M., Su, H., Yu, X., and Zhang, Y.: Mapping Asian anthropogenic emissions of non-methane volatile organic compounds to multiple chemical mechanisms, Atmos. Chem. Phys., 14, 5617–5638, doi:10.5194/acp-14-5617-2014, 2014.

Li, M., Zhang, Q., Kurokawa, J., Woo, J.-H., He, K., Lu, Z., Ohara, T., Song, Y., Streets, D. G., Carmichael, G. R., Cheng, Y., Hong, C., Huo, H., Jiang, X., Kang, S., Liu, F., Su, H. and Zheng, B.: MIX: a mosaic Asian anthropogenic emission inventory under the international collaboration framework of the MICS-Asia and HTAP, Atmospheric Chem. Phys., 17(2), 935–963, doi:10.5194/acp-17-935-2017, 2017.

Li, Z., Xia, X., Cribb, M, Mi,W., Holben,B., Wang, P., Chen, H., Tsay S. C., Eck, T. F., Zhao, F., Dutton, E. G., and Dickerson, R. E.: Aerosol optical properties and their radiative effects in northern China, J. Geophys. Res., 112, D22S01, doi:10.1029/2006JD007382, 2007.

Li, Z., Lee, K. H., Wang, Y., Xin, J., Hao, W.-M.: First observation based estimates of cloud free aerosol radiative forcing across China, J. Geophys. Res.-Atmos., 115(D7), 2010.

Liu X., Easter, R. C., Ghan, S. J., Zaveri, R., Rasch, P., Shi, X., Lamarque, J.-F., Gettelman, A., Morrison, H., Vitt, F., Conley, A., Park, S., Neale, R., Hannay, C., Ekman, A. M. L., Hess, P., Mahowald, N., Collins, W., Iacono, M. J., Bretherton, C. S., Flanner, M. G., and Mitchell, D.: Toward a minimal representation of aerosols in climate models: description and evaluation in the Community Atmosphere Model CAM5, Geosci. Model Dev., 5, 709–739, doi:10.5194/gmd-5-709-2012, 2012.

Liu, Y., Huang, J., Shi, G., Takamura, T., Khatri, P., Bi, J., Shi, J., Wang, T., Wang, X., and Zhang, B.: Aerosol optical properties and radiative effect determined from skyradiometer over Loess Plateau of Northwest China, Atmos. Chem. Phys., 11, 11455-11463, 2011.

Ohara, T., Akimoto, H., Kurokawa, J., Horii, N., Yamaji, K., Yan, X., and Hayasaka, T.: An Asian emission inventory of anthropogenic emission sources for the period 1980-2020, Atmos. Chem. Phys., 7, 4419–4444, doi:10.5194/acp-7-4419-2007, 2007.

Seinfeld, J. H. and Pandis, S. N.: Atmospheric chemistry and physics: from air pollution to climate change, John Wiley & Sons, 1998.

Shindell, D. T., Lamarque, J.-F., Schulz, M., Flanner, M., Jiao, C., Chin, M., Young, P. J., Lee, Y. H., Rotstayn, L., Mahowald, N., Milly, G., Faluvegi, G., Balkanski, Y., Collins, W. J., Conley, A. J., Dalsoren, S., Easter, R., Ghan, S., Horowitz, L., Liu, X., Myhre, G., Nagashima, T., Naik, V., Rumbold, S. T., Skeie, R., Sudo, K., Szopa, S., Takemura, T., Voulgarakis, A., Yoon, J.-H., and Lo, F.: Radiative forcing in the ACCMIP historical and future climate simulations, Atmos. Chem. Phys., 13(6), 2939-2974, 2013.

Tao, J., Zhang, L., Engling, G., Zhang, R., Yang, Y., Cao, J., Zhu, C., Wang, Y., and Luo, L.: Chemical composition of $PM_{2.5}$ in an urban environment in Chengdu, China: importance of springtime dust storms and biomass burning[, Atmos. Res., 122, 270-283, 2013.

Tao, J., Zhang, L., Ho, K., Zhang, R., Lin, Z., Zhang, Z., Lin, M., Cao, J., Liu, S., and Wang, G.: Impact of $PM_{2.5}$ chemical compositions on aerosol light scattering in Guangzhou-the largest megacity in South China, Atmos. Res, 135, 48-58, 2014.

Thomas G. E. and Stamnes K., Radiative Transfer in the Atmosphere and Ocean, Cambridge Press, 1999.

Xia, X., Chen, H., Goloub, P., Zhang, W., Chatenet, B., and Wang, P.: A complicaiton of aerosol optical properties and calculation of direct radiative forcing over an urban region in northern China, J. Geophy. Res., 112, d12203, doi:10.1029/2006JD008119, 2007a.

Xia, X., Chen, H., Li, Z., Wang, P., and Wang J.: Significant reduction of surface solar irradiance induced by aerosols in a suburban region in northeastern China, J. Geophys. Res., 112, doi:10.1029/2006JD007562, 2007b.

Xia, X., Li, Z., Holben, B., Wang, P., Eck, T., Chen, H., Cribb, M., and Zhao, Y.: Aerosol optical properties and radiative effects in the Yangtze Delta region of China, J. Geophys. Res., 112, D22S12, 2007c.

Xin, J., Wang, Y., Li, Z., Wang, P., Hao, W., Nordgren, B. L., Wang, S., Liu, G., Wang, L., Wen, T., Sun, Y., and Hu, B.: Aerosol optical depth (AOD) and Ångström exponent of aerosols observed by the Chinese Sun Hazemeter Network from August 2004 to September 2005, J. Geophys. Res.-Atmos., 112, D05203, doi:10.1029/2006JD007075, 2007.

Zhang, F., Xu, L., Chen, J., Yu, Y., Niu, Z., and Yin, L.: Chemical compositions and extinction coefficients of $PM_{2.5}$ in peri-urban of Xiamen, China, during June 2009–May 2010, Atmos. Res., 106, 150-158, 2012.

Zhang F., Wang Z., Cheng H., Lv X., Gong W., Wang, X., Zhang G. Seasonal variations and chemical characteristics of PM2.5 in Wuhan, central China, Sci. Total Environ., 518–519, 97–105, 2015.

Zhang, K., Wan, H., Liu, X., Ghan, S. J., Kooperman, G. J., Ma, P.-L., Rasch, P. J., Neubauer, D., and Lohmann U.: Technical Note: On the use of nudging for aerosol–climate model intercomparison studies, Atmos. Chem. Phys., 14(16),8631-8645, 2014.

Zhang, R., Jing, J., Tao, J., Hsu, S.-C., Wang, G., Cao, J., Lee, C. S. L., Zhu, L., Chen, Z., Zhao, Y., and Shen, Z.: Chemical characterization and source apportionment of $PM_{2.5}$ in Beijing: seasonal perspective, Atmos. Chem. Phys., 13(14), 7053-7074, 2013.

Zhao, P. S., Dong, F., He, D., Zhao, X. J., Zhang, X. L., Zhang, W. Z., Yao, Q., and Liu, H. Y.: Characteristics of concentrations and chemical compositions for $PM_{2.5}$ in the region of Beijing, Tianjin, and Hebei, China, Atmos. Chem. Phys., 13, 4631-4644, 2013.

Zhuang, B.L., Wang, T.J., Li, S., Liu, J., Talbot, R., Mao, H.T., Yang, X.Q., Fu, C.B., Yin, C.Q., Zhu, J. L., Che, H.Z., and Zhang, X.Y.: Optical properties and radiative forcing of urban aerosols in Nanjing, China, Atmos. Environ., 83, 43-52, 2014.